BUSING, W. R. & LEVY, H. A. (1967). Angle calculations for 3- and 4-circle X-ray and neutron diffractometers. *Acta Cryst.* **22**, 457-464.
DIAMOND, R. (1969). Profile analysis in single crystal diffractometry. *Acta Cryst.* **25**, 43-55.
DIRAC, P. A. M. (1958). *The Principles of Quantum Mechanics*, 4th ed., §§ 5-6, pp. 14-22 (bra-ket notation) and § 15, pp. 58-61 (delta function). Oxford Univ. Press.
EWALD, P. P. (1913). Zur Theorie der Interferenzen der Röntgenstrahlen in Kristallen. *Phys. Z.* **14**, 465-472.
KABSCH, W. (1988). Evaluation of single-crystal X-ray diffraction data from a position-sensitive detector. *J. Appl. Cryst.* **21**, 916-924.
LIPSON, H. (1972). *International Tables for X-ray Crystallography*, Vol. II, p. 265, equations (11). Birmingham: Kynoch Press. (Present distributor Kluwer Academic Publishers, Dordrecht.)
MOORE, E. H. (1920). On the reciprocal of the general algebraic matrix [abstract]. *Bull. Am. Math. Soc.* **26**, 394-395.
MOORE, E. H. (1935). *General Analysis*. Philadelphia: American Philosophical Society.
PENROSE, R. (1955). A generalized inverse for matrices. *Proc. Cambridge Philos. Soc.* **51**, 406-413.
RICHMOND, T. J., FINCH, J. T., RUSHTON, B., RHODES, D. & KLUG, A. (1984). Structure of the nucleosome core particle at 7 Å resolution. *Nature (London)*, **311**, 532-537.
THOMAS, D. J. (1982). Fast diffractometry. PhD thesis, Cambridge Univ., England.
THOMAS, D. J. (1989). Calibrating an area-detector diffractometer: imaging geometry. *Proc. R. Soc. London Ser. A*, **425**, 129-167.
THOMAS, D. J. (1990*a*). Calibrating an area-detector diffractometer: integral response. *Proc. R. Soc. London Ser. A*, **428**, 181-214.
THOMAS, D. J. (1990*b*). Modern equations of diffractometry. Goniometry. *Acta Cryst.* A**46**, 321-343.
THOMAS, D. J. (1992). Modern equations of diffractometry. Diffraction geometry. *Acta Cryst.* A**48**, 134-158.
WONACOTT, A. J. (1977). Geometry of the rotation method. *The Rotation Method in Crystallography*, edited by U. W. ARNDT & A. J. WONACOTT, ch. 7, pp. 75-103. Amsterdam: North-Holland.

Acta Cryst. (1993). A**49**, 460-467

Simulation of X-ray Topographs: a New Method to Calculate the Diffracted Field

BY C. A. M. CARVALHO AND Y. EPELBOIN

Laboratoire de Minéralogie-Cristallographie, Universités P. M. Curie et Paris VII, *UA* 009, *CNRS, Case* 115, 75252 *Paris CEDEX* 05, *France*

(*Received* 21 *July* 1992; *accepted* 8 *October* 1992)

Abstract

The precision of the numerical algorithms used to integrate the Takagi-Taupin equations has been in the past a severe limitation for the simulation of accurate topographs. The intensity, especially in the direct image of the defect, is underestimated. This has forbidden the use of the reciprocity theorem for the simulation of traverse and white-beam synchrotron topographs. A new algorithm is described, based on two different methods of expressing the partial-derivative equations, which permits a faster and more accurate calculation.

I. Introduction

X-ray topography is a widespread method for single-crystal characterization. Computer simulation of topographs is useful for image interpretation because it allows quantitative analysis of the perfection of crystals. The comparison between the computed and the experimental images makes it possible to test the validity of a deformation model for the defects seen in the image and to determine quantitatively parameters that are not accessible through the experiment such as the sign and magnitude of the Burgers vector of a dislocation or the nature of a stacking fault. Simulation of section topographs is now well established (Epelboin, 1985). As for traverse topographs, Petrashen, Chukovskii & Shulpina (1980) have attempted to calculate the intensity along a line of the image and Epelboin & Soyer (1985) have simulated whole images. The latter have shown that the precision of the algorithms was not sufficient for the reciprocity theorem of optics to be used as suggested by Petrashen (1976).

Three aspects must be considered when computing X-ray topographs:

(i) the kind of wave incident on the surface of the crystal;

(ii) the numerical method to solve the propagation equations inside the crystal;

(iii) the network of integration used to integrate these equations.

Let us briefly review each of them. X-ray topography may be classified into two groups: plane-wave and spherical-wave topography. Laboratory and synchrotron-radiation sources produce spherical waves (Aristov, Kohn, Polovinkina & Snigirev, 1982; Carvalho & Epelboin, 1990), so that to obtain a plane wave it is necessary to put a specially designed monochromator in front of the specimen. Petrashen *et al.* (1980) explained why the most efficient method to simulate plane-wave topographs is the Tournarie method (Authier, Malgrange & Tournarie, 1968). Thus, in this paper we will study only the case of the spherical wave, *i.e.* section and traverse topographs.

0108-7673/93/030460-08$06.00

The contrast may be explained as the addition of the intensities produced by independent point sources distributed along the entrance surface of the crystal (Aristov *et al.*, 1982). This is also true for synchrotron topography, in spite of the usually large source-to-crystal distance (Carvalho & Epelboin, 1990). The reason for this is the small coherence length of the incident radiation. X-rays produced by a point source propagate in the crystal inside the Borrmann triangle. This means that the simulation of section, traverse or synchrotron topographs consists mainly in the calculation of the X-ray field inside the Borrmann fan along a network of integration (Fig. 1).

Three numerical methods have so far been used for this calculation. Petrashen (1976) proposed a method to calculate the diffracted field only. In this method, it is necessary to evaluate $\exp(i2\pi\mathbf{h}\cdot\mathbf{u})$ at each step of the computation, where $\mathbf{h}$ is the reciprocal-lattice vector and $\mathbf{u}$ is the displacement due to the deformation at a given point inside the crystal. The evaluation of a complex exponential takes a long time and it dramatically slows down the integration process. Epelboin (1981) and Epelboin & Soyer (1985) used a method established by Tournarie (Authier *et al.*, 1968) to simulate section and traverse topographs. This method has the advantage of evaluating a derivative of $\mathbf{h}\cdot\mathbf{u}$ instead of the complex exponential, which is much faster. However, both the diffracted and the transmitted fields must be calculated at each node of the network. This feature unnecessarily increases the number of arithmetic operations. If either the diffracted or the reflected field is known, the other is available by a simple calculation by means of one of the Takagi–Taupin equations (Takagi, 1969). Taupin (1967) used another method, which should give better precision. However, it is necessary to evaluate the deformation at several nodes for each step of integration and this requires a greater number of arithmetic operations. As a consequence, Nourtier & Taupin (1981) found that this method is slower, for a given precision, than the Tournarie method.

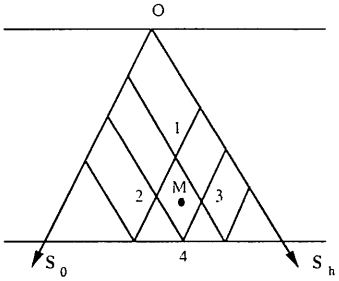

Fig. 1. Principle of the network of integration. *O*: point source along the entrance surface of the crystal; $\mathbf{s}_0$ and $\mathbf{s}_h$ are the refracted and reflected directions, respectively. 1, 2, 3, 4 are four nodes of the network, which define a cell of integration.

Another aspect of the simulation procedure is the choice of the network of integration. Epelboin (1981) suggested an algorithm for its construction based on the width of the extinction fringes for a perfect crystal. Since the established network is often not dense enough in the most deformed areas, he used a procedure valid only for dislocations, which decreases the integration steps in the region around the direct image of the dislocation. Up to now, no general algorithm of refinement of the integration network, applicable to any kind of deformation, has been proposed.

In this paper, we present a new method to calculate the diffracted field. It is faster because it combines the advantages of both previous methods. We first explain its basic principles and then discuss its application to the computation of the diffracted intensity. In the last section, we present a new method to refine the integration network that may be applied to any kind of deformation and not only to dislocations.

In a second paper (Carvalho & Epelboin, 1993), we will explain the use of this algorithm for the simulation of traverse and synchrotron topographs. Since its precision is better than the previous ones, it allows the use of the reciprocity theorem and this reduces the computation time.

II. The diffraction equations

As previously explained, we are interested in the computation of the diffracted amplitude $D_h(\mathbf{r})$ only, since the refracted intensity may be deduced from its value. It may be written as (Takagi, 1969)

$$D_h(\mathbf{r}) = \tilde{\Psi}(\mathbf{r})\exp[+i2\pi\mathbf{h}\cdot\mathbf{u}(\mathbf{r})] \times \exp[-i2\pi(\mathbf{k}_0+\mathbf{h})\cdot\mathbf{r}],$$

where $\mathbf{r}$ is the position vector of a point in the crystal and $\mathbf{k}_0$ is the direction of the incident wave. Since Takagi's equations give the freedom to choose the extremity of the incident wave vector, we choose $\mathbf{k}_0$ so that $|\mathbf{k}_0| = |\mathbf{k}_0+\mathbf{h}|$. The equation that describes the amplitude in the crystal becomes (Takagi, 1969)

$$\partial^2\tilde{\Psi}/\partial s_0\partial s_h + i2\pi(\partial\mathbf{h}\cdot\mathbf{u}/\partial s_h)(\partial\tilde{\Psi}/\partial s_0) + [\pi^2K^2C^2\chi_h\chi_{\bar{h}} + i2\pi(\partial^2\mathbf{h}\cdot\mathbf{u}/\partial s_0 s_h)]\tilde{\Psi} = 0. \quad (1)$$

s_0 and s_h are the coordinates along the refracted and diffracted directions, respectively (Fig. 2), $K = 1/\lambda$, where λ is the wavelength of the X-rays, and χ_h is the hth Fourier coefficient of the polarizability of the crystal. $C = 1$ or $\cos 2\theta$ for σ or π polarization, respectively, and θ is the Bragg angle.

To specify $\tilde{\Psi}$ completely, we must write the boundary conditions. The values of $\tilde{\Psi}(r)$ along the edges of the Borrmann triangle may be determined from the Riemann function (Takagi, 1969):

$$\tilde{\Psi}(P) = F\int_{BA}\gamma_0(\zeta)v(P,\xi)\Phi_0(\xi)\,\mathrm{d}\xi,$$

where P is a point along the exit surface of the crystal (Fig. 2), BA is the base of the Borrmann triangle along the entrance surface, $\gamma_0 = \cos\varphi_0$ where φ_0 is the angle between the normal to the entrance surface and the $\mathbf{s}_0$ direction, v is the Riemann function and Φ_0 is the amplitude of the incident wave multiplied by a phase factor $F = -i\pi KC\chi_h/\sin 2\theta$. For a point wave incident at point Q along BA, $\Phi_0 = \delta(\xi-\xi_Q)/\gamma(\xi)$, so that the diffracted field produced by such a source on the exit surface is proportional to $v(P, Q)$. Along the segment PA, $v = 1$ for any point P, which means that $\tilde{\Psi} = F$ along QB'. Along PB, $v(P, s_0, s_h) = \exp\{-i2\pi\mathbf{h}\cdot[\mathbf{u}(s_0, s_h) - \mathbf{u}(P)]\}$. This means that the field created by a point source at point Q is defined by the boundary conditions

$$\tilde{\Psi}_Q(P) = F \quad \text{along } \mathbf{s}_0,$$
$$\tilde{\Psi}_Q(P) = F\exp\{-i2\pi\mathbf{h}\cdot[\mathbf{u}(P) - \mathbf{u}(Q)]\} \quad \text{along } \mathbf{s}_h. \tag{2}$$

Now let us define two new amplitudes, Ψ and Φ, by the relations

$$\exp[+i2\pi\mathbf{h}\cdot\mathbf{u}(s_0, s_h)]\tilde{\psi} = F\exp[+i2\pi\mathbf{h}\cdot\mathbf{u}(s_0, s_{hQ})]\psi, \tag{3}$$
$$\tilde{\psi} = F\exp\{-i2\pi\mathbf{h}\cdot[\mathbf{u}(s_{0Q}, s_h) - \mathbf{u}(Q)]\}\Phi.$$

From (2), it is easy to see that the boundary conditions Φ and Ψ are

$$\Phi = \Psi = 1 \quad \text{along } \mathbf{s}_0 \text{ and } \mathbf{s}_h.$$

The propagation equations for Φ and Ψ are readily obtained from (1):

$$\partial^2\Psi/\partial s_0\partial s_h + W_\psi\partial\Psi/\partial s_h + \pi^2K^2C^2\chi_h\chi_{\bar{h}}\Psi = 0 \tag{4}$$

with

$$W_\Psi = -i2\pi[(\partial\mathbf{h}\cdot\mathbf{u}/\partial s_0)(s_0, s_h) - (\partial\mathbf{h}\cdot\mathbf{u}/\partial s_0)(s_0, 0)]$$

and

$$\partial^2\Phi/\partial s_0\partial s_h + W_\Phi\partial\Phi/\partial s_0 + (\pi^2K^2C^2\chi_h\chi_{\bar{h}} + \partial W_\Phi/\partial s_0)\Phi = 0 \tag{5}$$

with

$$W_\Phi = i2\pi[(\partial\mathbf{h}\cdot\mathbf{u}/\partial s_h)(s_0, s_h) - (\partial\mathbf{h}\cdot\mathbf{u}/\partial s_h)(0, s_h)].$$

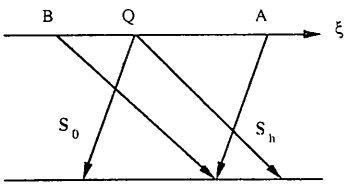

Fig. 2. Coordinates used in the integration process. $\mathbf{s}_0$ and $\mathbf{s}_h$ are the refracted and diffracted directions. ζ is an axis along the entrance surface of the crystal.

For the numerical calculation, we use either Ψ or Φ, as explained in the next section. They give the same value for the intensity, since they only differ by a phase factor.

III. Numerical methods

To solve the propagation equations, we divide the Borrmann triangle along a set of lines parallel to the $\mathbf{s}_0$ and $\mathbf{s}_h$ axes (Fig. 1). This defines a network of integration with steps p and q along $\mathbf{s}_0$ and $\mathbf{s}_h$, respectively. To obtain a numerical formula suitable for the computation, we integrate the propagation equation over a cell in the network (Fig. 1).

Let us first consider (4). For the first term, we may write

$$\int_{\text{cell}} (\partial^2\psi/\partial s_0\partial s_h)\,ds_0 ds_h = \psi_4 - \psi_3 - \psi_2 + \psi_1, \tag{6}$$

where the subscript of Ψ indicates the point of the cell where it is calculated (Fig. 1).

Let us now consider the third term in (4). It is easy to show by a Taylor-series expansion that, for a general function f,

$$\int_a^b f(x)\,dx \simeq f[(a+b)/2](b-a) + [(b-a)^3/24]f''[(a+b)/2] \simeq [(b-a)/2][f(a)+f(b)] - [(b-a)^3/12]f''[(a+b)/2]. \tag{7}$$

Thus, we may write

$$\int_{\text{cell}} \Psi\,ds_0 ds_h \simeq (pq/4)(\Psi_4+\Psi_3+\Psi_2+\Psi_1) - (p^3q/12)(\partial^2\Psi/\partial s_0^2)_M - (pq^3/12)(\partial^2\Psi/\partial s_h^2)_M. \tag{8}$$

Here, M means the centre of the integration cell (Fig. 1).

To integrate the second term of (4), we use the first form of (7) along $\mathbf{s}_0$ and $\mathbf{s}_h$,

$$\int_{\text{cell}} W_\Psi(\partial\Psi/\partial s_h)\,ds_0 ds_h \simeq pq(W_\Psi\partial\Psi/\partial s_h)_M + (p^3q/24)(\partial^2/\partial s_0^2)(W_\Psi\partial\Psi/\partial s_h)_M + (pq^3/24)(\partial^2/\partial s_h^2)(W_\Psi\partial\Psi/\partial s_h)_M.$$

To express $\partial\Psi/\partial s_h$ as a function of the values of Ψ at the vertices of the cell, we use the approximation

$$f'(x) \simeq \{f[x+(b-a)/2] - f[x-(b-a)/2]\}/(b-a) - [(b-a)^2/24]f'''(x).$$

Thus,

$$\int_{\text{cell}} W_\Psi(\partial\Psi/\partial s_h)\,ds_0 ds_h \simeq (p/2)W_\Psi(M)(\Psi_4+\Psi_3-\Psi_2-\Psi_1) + (p^3q/8)[\tfrac{1}{3}(\partial^2/\partial s_0^2)(W_\Psi\partial\Psi/\partial s_h)_M - (W_\Psi\partial^3\Psi/\partial s_0^2\partial s_h)_M] + (pq^3/24)[(\partial^2 W_\Psi/\partial s_h^2)(\partial\Psi/\partial s_h) + 2(\partial W_\Psi/\partial s_h)(\partial^2\Psi/\partial s_h^2)]_M. \quad (9)$$

Substituting (6), (8) and (9) into (4), we finally obtain

$$[1+(p/2)W_\Psi(M)+(pq/4)G]\Psi_4 = \Psi_3+\Psi_2-(p/2)W_\Psi(M)(\Psi_3-\Psi_2-\Psi_1) - (pq/4)G(\Psi_3+\Psi_2+\Psi_1)+\varepsilon_\Psi, \quad (10)$$

where

$$G=\pi^2K^2C^2\chi_h\chi_{\bar h}$$

$$\varepsilon_\Psi = -(p^3q/8)[\tfrac{1}{3}(\partial^2/\partial s_0^2)(W_\Psi\partial\Psi/\partial s_h) - W_\Psi\partial^3\Psi/\partial s_0^2\partial s_h - \tfrac{2}{3}(\partial^2\Psi/\partial s_0^2)G]_M - (pq^3/12)[\tfrac{1}{2}(\partial^2 W_\Psi/\partial s_h^2)(\partial\Psi/\partial s_h) + (\partial W_\Psi/\partial s_h - G)(\partial^2\Psi/\partial s_h^2)]_M.$$

From (5), it is possible to calculate Φ in a similar way,

$$[1+(p/2)W_\Phi(s_0,s_{hm})+(pq/4)G]\Phi_4 = \Phi_3+\Phi_2-\Phi_1-(pq/4)G(\Phi_3+\Phi_2+\Phi_1) - (q/2)W_\Phi(s_0,s_{hm})(\Phi_2+\Phi_1) + (q/2)W_\Phi(s_0-p,s_{hm})(\Phi_3+\Phi_1)+\varepsilon_\Phi \quad (11)$$

with

$$\varepsilon_\Phi = (p^3q/12)G(\partial^2\Phi/\partial s_0^2)_M + (q^3/8)\Delta(W_\Phi\partial^2\Phi/\partial s_h^2 - \tfrac{1}{3}\partial^2 W_\Phi/\partial s_h^2 + \tfrac{2}{3}G\partial^2\Phi/\partial s_h^2). \quad (12)$$

Here, $\Delta(X)=X(s_0,s_{hm})-X(s_0-p,s_{hm})$ and $s_{hm}=s_h-q/2$.

Equations (10) and (11) may be written in a form that minimizes the number of arithmetic operations. By a suitable factorization, we find

$$\psi_4=[(Q_\psi-\tilde G)\psi_3-(Q_\psi+\tilde G)(\psi_2+\psi_1) + \psi_2+\psi_2]/(Q_\psi^*+\tilde G), \quad (13)$$

$$\Phi_4=[(Q_\Phi^*-\tilde G)\Phi_2+(Q_a+\tilde G)(\Phi_3+\Phi_1) - \Phi_1-\Phi_1]/(Q_\Phi+\tilde G), \quad (14)$$

with

$$Q_\Psi=1-(p/2)W_\Psi(M)$$
$$Q_\Phi=1+(q/2)W_\Phi(s_0,s_{hm})$$
$$\tilde G=(pq/4)\pi^2K^2C^2\chi_h\chi_{\bar h}$$
$$Q_a=1+(q/2)W_\Phi(s_0-p,s_{hm}).$$

To compute the field at any point in the network, one has to perform one complex division, two multiplications and seven additions or subtractions. By an appropriate manipulation of the Tournarie formula, it can be shown that this method needs two divisions, six multiplications and five addition or subtractions. Thus, the new method is much faster. From now on we will refer to (13) and (14) as the Ψ and the Φ methods, respectively.

IV. Error-convergence analysis

Some insight into the behaviour of these two numerical methods may be gained from their error terms. The coefficient of p^3q in the expression for ε_Φ is much simpler than that in the expression for ε_Ψ. The former does not depend explicitly on the deformation and contains the second derivative of Φ, while the latter contains third-order derivatives of $\mathbf{h}\cdot\mathbf{u}$ and Ψ. In strongly deformed regions, the amplitudes Ψ and Φ vary rapidly, so that their successive derivatives increase in magnitude. We may expect the coefficient of p^3q in ε_Ψ to be larger than that of ε_Φ. This means that (13) (the Ψ method) is more sensitive to the size of the step p than (14) (the Φ method), since p^3q depends mostly on p. This is confirmed by our simulations.

Fig. 3 presents the geometry of a dislocation in quartz that we have used as a test. It was also studied by Epelboin & Patel (1982) and we know that the quality of this image is very sensitive to the accuracy of the simulation. This is due to the large magnitude of the stress field around the dislocation. Fig. 4 presents the simulation of this dislocation in a section topograph. In Fig. 4(*c*), it has been computed with the Tournarie method and use of the network established by Epelboin (1981): the values of p and q vary inside the Borrmann fan according to the position of the extinction fringes in the corresponding perfect crystal. The sampling of the nodes follows as closely as possible the variation of the amplitude: there are

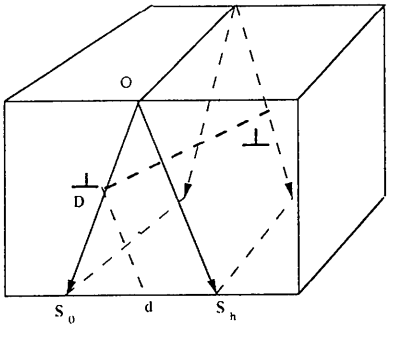

Fig. 3. Geometry of the dislocation simulated in the section topograph in Fig. 4 (Epelboin & Patel, 1982). The dislocation *D* lies parallel to the surface. *d* indicates the position of the direct image.

more nodes near the edges, where the amplitude varies rapidly. This network is called the 'standard network'. In Figs. 4(*a*) and (*b*), we use the same network of integration but with the Ψ and Φ methods, respectively. Figs. 4(*b*) and (*c*) are similar, except in the dynamical image, which is seen most clearly in Fig. 4(*b*). This is in closest agreement with the experiment. When using the Ψ method, an error appears clearly in Fig. 4(*a*) as a black horizontal contrast in the region where a direct image exists. It arises from the areas where the dislocation is close to the transmitted beam (marked *D* in Fig. 3). In Fig. 5, the same image is computed using a standard network where the steps of integration have been decreased by a factor 8 and thus the computation time is about 64 times longer. The Φ and Ψ methods give the same image and the results are in very good agreement with the experiment but the computation times are not acceptable. From Fig. 4, we may conclude that, to a limited precision, the Φ method behaves roughly like the Tournarie method.

(*a*)

(*b*)

(*c*)

Fig. 4. Simulation of a dislocation in quartz. Geometry shown in Fig. 3. Ag $K\alpha$, $0\bar{1}.\bar{1}$ reflection (Epelboin & Patel, 1982). (*a*) Ψ method, (*b*) Φ method, (*c*) Tournarie method.

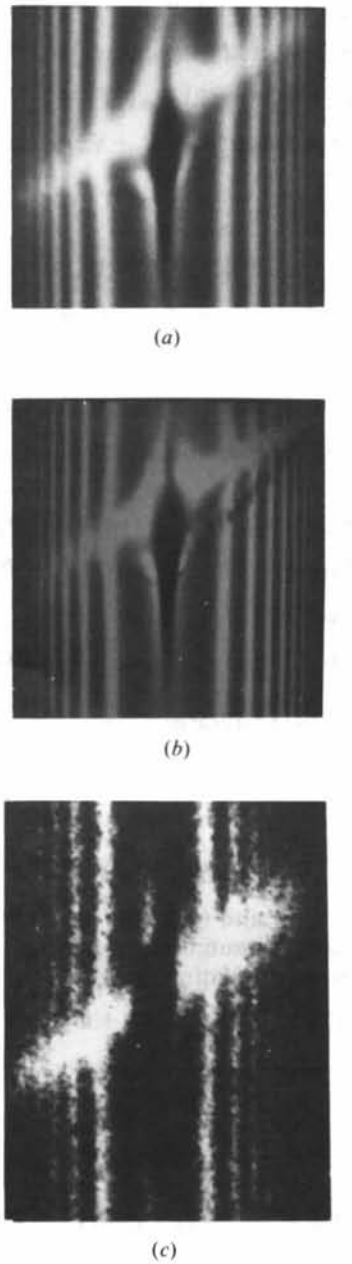

(*a*)

(*b*)

(*c*)

Fig. 5. Same as Fig. 4, except the steps of integration are eight times smaller. (*a*) Ψ method, (*b*) Φ method, (*c*) experimental image.

The error term for the diffracted field in the Tournarie method is

$$\delta_\Phi = \pi^2 K^2 C^2 \chi_h \chi_{\bar{h}} (\rho^3 q/24)(\partial^2 T_h/\partial s_0^2) + (q^3/8)[-\tfrac{2}{3} i\pi K C \chi_{\bar{h}} \partial^2 T_0/\partial s_h^2 + \tfrac{1}{3}\partial^2(WT_h)/\partial s_h^2 + W\partial^2 T_h/\partial s_h^2],$$

where T_0 and T_h are the refracted and diffracted amplitudes. We note that it resembles the error expressed in (12). We may then expect that the Φ method behaves similarly to the Tournarie method, as seen in Figs. 4(b) and (c).

Let us now consider the second part of the error terms. The coefficient of pq^3 in ε_Ψ includes third-order derivatives of $\mathbf{h}\cdot\mathbf{u}$. At first sight, this is also the case for the coefficient of q^3 in ε_Φ but Δ means that the coefficient is the difference between the terms in the parentheses calculated at two points separated by a distance p. In the case of a dislocation, the higher derivatives of W are large in a small region near the core since $W \simeq 1/r$, r being the distance from the computed point to the core. When the steps are not too small, the sampling of the nodes may avoid the core and these higher-order terms will remain small enough so that the error is acceptable. However, this may no longer be the case for a denser network. When the steps p are small, we may use the approximation $\Delta(X) \simeq p\partial X/\partial s_0$, thus, fourth-order derivatives appear in the coefficient of pq^3, which becomes large. We may conclude that the Φ method tends to give better results for a moderately dense network but may have a non-uniform convergence and may give worse results than the Ψ method for a more refined network in the case of localized deformations such as dislocations. The Tournarie method should be less sensitive because there is no Δ term in the error expression. However, when the network is not too dense, we may expect the Φ method to be more precise than the Tournarie method. This is confirmed in the simulations in Fig. 4.

Fig. 7 is the simulation of the same dislocation but using a refined network of integration, as drawn in Fig. 6. In this case, the integration steps are small in the vicinity of the core of the defect and ε_Φ may become large at the nodes near the core where the amplitude is computed. The image in Fig. 7(a) is better than that in Fig. 7(b), showing that the Ψ method gives better results when decreasing the step size than the Φ method. Comparing these images with those in Fig. 4, we see that the Φ method does not converge uniformly with a reduction of the step size while the Ψ method does. This confirms our theoretical explanation.

The error terms are an estimation of the local error, which appears when going from one point of the network to the next. Unfortunately, it is not possible to evaluate it at each step of the calculation to check if the integration step is small enough. This is sometimes used for ordinary differential equations but in

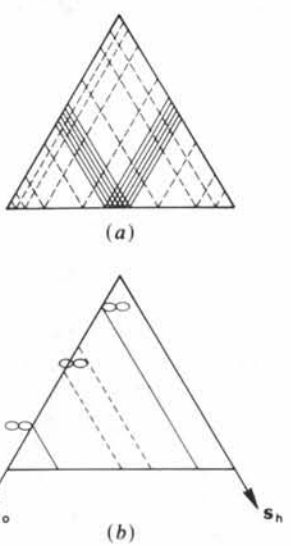

(a)

(b)

Fig. 6. Schematic drawing of a refined network of integration in the case of a dislocation. (a) The steps p and q are made smaller in the areas where the dislocation intersects the transmitted beam, thus the density of nodes is larger in the directions corresponding to the propagation of the corresponding beam (Epelboin, 1981). (b) The dashed lines show the refined region in a given incidence plane. The solid lines show the limits where the refinement is used.

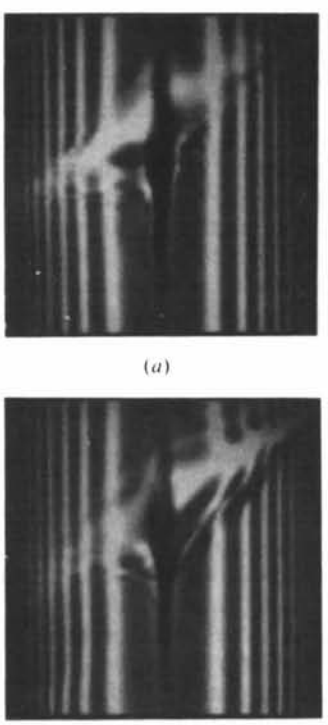

(a)

(b)

Fig. 7. Same dislocation as in Fig. 5 but using a refined network where the direct image originates. (a) Ψ method, (b) Φ method.

the present case it would slow down the computation time and this is not acceptable. Furthermore, the local errors give a qualitative comprehension of the behaviour of the method but it is not possible to predict quantitatively the propagation of the total error during the integration, especially for hyperbolic equations such as (4) and (5). It is necessary to test the adequacy of the network through simulations for each physical problem, *i.e.* for any kind of material, deformation and reflection.

V. Simulation of section topographs

The basic principle of the 'standard network' introduced by Epelboin (1981) is that the sampling of the nodes in the integration network is calculated and follows, as closely as possible, the variations of the amplitude in the Borrmann fan: there are more nodes near the edges where the amplitude varies rapidly and also, optionally (the 'refined network'), in the areas where the defect intersects the $\mathbf{s}_0$ direction, *i.e.* where the direct image originates.

From the previous discussion, we may assume that the Ψ method gives satisfactory results everywhere except in a well defined area between the direct image and the transmitted beam (Fig. 4*a*). In this region, the integration steps must be reduced to obtain a satisfactory image (Fig. 7*a*). Therefore, a refined network (Fig. 6) must be used, which means that the computation time is increased. The Φ method is less sensitive to the step size but does not give the same quality as the Ψ method between the direct image and the diffracted beam and has a nonuniform convergence, which is a problem when one wants to increase the precision of the calculation.

The building of the refined part of the network as shown in Fig. 6 is specific to a dislocation, so we have tried to establish a method of computation valid for any kind of deformation. Since in the most deformed areas the coupling between the refracted and reflected beams is weak, they propagate nearly independently. We have therefore assumed that the most deformed areas behave like an amorphous material but this leads to very poor images.

It is clear that the Ψ and Φ methods present complementary features. We have found that the best solution is to use both to calculate an image. In the lines where the Ψ method is not satisfactory, we use it only for the nodes between the direct image and the diffracted beam and use the Φ method for the other nodes. The switching between the two methods is made automatically using the criterion of validity of the geometrical optics (Balibar, 1969): since the error depends on the value of the deformation near the transmitted direction $\mathbf{s}_0$, which is related to the amount of newly created wavefields, we compare $\partial^2\mathbf{h}\cdot\mathbf{u}/\partial s_0\partial s_h$ to $\pi^2K^2C^2\chi_h\chi_{\bar{h}}$ to decide where to switch between the two methods. This gives a very

Fig. 8. Same dislocation as in Fig. 5 but using an automatic switching between the Φ and Ψ methods.

(*a*)

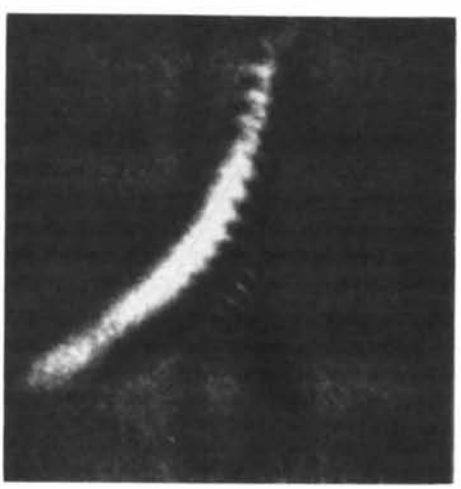

(*b*)

Fig. 9. Simulation of a dislocation in silicon, Mo $K\alpha$, 220 reflection. Compare this simulation with the result from using the Tournarie method given by Epelboin (1981). (*a*) Experimental image, (*b*) simulation.

satisfactory image (Fig. 8). An example of a dislocation in silicon is shown in Fig. 9.

This automatic switching cannot be used for extended defects, since it is not possible to establish a refined network as shown in Fig. 6: the defect intersects the transmitted beam in all planes of incidence and one must rebuild a different refined network for each incidence plane. The best method is to use the Φ method for the nodes between the direct image and $\mathbf{s}_h$ and the Ψ method near $\mathbf{s}_0$. The only difficulty is that one must switch between the integration formulae (13) and (14). This means, as indicated in (3), that one must change the phase of the wave in the middle of the integration process. This may be rather delicate since the phase between two adjacent nodes in the integration network may vary more rapidly than the modulus of the amplitudes. This means that one must be very careful about the length of the steps of integration. No general values can be given since it depends on the kind of material and deformation and only a trial-and-error method maybe used. We have used this method to simulate the images of quartz piezoelectric resonators and we found after many tests that the step sizes could be used for all the simulations independently from the diffraction parameters (Carvalho, 1990).

Concluding remarks

In the present paper, we describe a new numerical algorithm to integrate Takagi–Taupin equations when the incident wave is not a plane wave. We have been able to estimate the error term and minimize it by using two different forms of the equations in the numerical computation. This new method presents two advantages.

(i) It is more accurate than the usual Tournarie method. As we will show in our next paper (Carvalho & Epelboin, 1993), it allows use of the theorem of reciprocity to simulate traverse and synchrotron topographs, which has not been possible before. There are many advantages to this, which will be explained in this paper.

(ii) It is faster since it needs less operations. The computing time is halved. It is now possible to compute section topographs on a good modern microcomputer. An image may be calculated in a few minutes and requires only a modest-size memory.

This method enables the simulation of section and traverse topographs to cover extended defects since now the simulation of the direct image is much more satisfactory.

CAMC acknowledges a doctorate scholarship from CNPq, Brazil.

References

ARISTOV, V. V., KOHN, V., POLOVINKINA, V. I. & SNIGIREV, A. A. (1982). *Phys. Status Solidi A*, **72**, 483-491.
AUTHIER, A., MALGRANGE, C. & TOURNARIE, M. (1968). *Acta Cryst.* A**24**, 126-136.
BALIBAR, F. (1969). *Acta Cryst.* A**25**, 650-658.
CARVALHO, C. A. M. (1990). Thesis, Univ. P. M. Curie, Paris, France.
CARVALHO, C. A. M. & EPELBOIN, Y. (1990). *Acta Cryst.* A**46**, 449-459.
CARVALHO, C. A. M. & EPELBOIN, Y. (1993). *Acta Cryst.* A**49**, 467-473.
EPELBOIN, Y. (1981). *Acta Cryst.* A**37**, 132-133.
EPELBOIN, Y. (1985). *Mater. Sci. Eng.* **73**, 1-43.
EPELBOIN, Y. & PATEL, J. R. (1982). *J. Appl. Phys.* **53**, 271-275.
EPELBOIN, Y. & SOYER, A. (1985). *Acta Cryst.* A**41**, 67-72.
NOURTIER, C. & TAUPIN, D. (1981). *J. Appl. Cryst.* **14**, 432-436.
PETRASHEN, P. V. (1976). *Sov. Phys. Solid State*, **18**, 2175-2176.
PETRASHEN, P. V., CHUKHOVSKII, F. N. & SHULPINA, I. L. (1980). *Acta Cryst.* A**36**, 287-295.
TAKAGI, S. (1969). *J. Phys. Soc. Jpn*, **26**, 1239-1253.
TAUPIN, D. (1967). *Acta Cryst.* **23**, 25-35.

Acta Cryst. (1993). A**49**, 467-473

Simulation of X-ray Traverse Topographs and Synchrotron Laue Topographs: Application of the Reciprocity Theorem

BY C. A. M. CARVALHO AND Y. EPELBOIN

Laboratoire de Minéralogie-Cristallographie, Universités P. M. Curie et Paris VII, *UA* 009, *CNRS, Case* 115, 75252 *Paris CEDEX* 05, *France*

(*Received* 21 *July* 1992; *accepted* 8 *October* 1992)

Abstract

A new demonstration of the reciprocity theorem of optics in the case of the X-ray dynamical theory is given. It is applied to the simulation of traverse and white-beam synchrotron topographs. It is shown that the accuracy of a new numerical algorithm [Carvalho & Epelboin (1993). *Acta Cryst.* A**49**, 460-467] allows

0108-7673/93/030467-07$06.00